Dynamical Mechanism for Sharp Orientation Tuning in an Integrate-and-Fire Model of a Cortical Hypercolumn

P. C. Bressloff
Nonlinear and Complex Systems Group, Department of Mathematical Sciences, Loughborough University, Loughborough, Leicestershire LE11 3TU, U.K.

N. W. Bressloff
Computational and Engineering Design Centre, Department of Aeronautics and Astronautics, University of Southampton, Southampton, SO17 1BJ, U.K.

J. D. Cowan
Department of Mathematics, University of Chicago, Chicago, IL 60637, U.S.A.

Orientation tuning in a ring of pulse-coupled integrate-and-fire (IF) neurons is analyzed in terms of spontaneous pattern formation. It is shown how the ring bifurcates from a synchronous state to a non-phase-locked state whose spike trains are characterized by clustered but irregular fluctuations of the interspike intervals (ISIs). The separation of these clusters in phase space results in a localized peak of activity as measured by the time-averaged firing rate of the neurons. This generates a sharp orientation tuning curve that can lock to a slowly rotating, weakly tuned external stimulus. Under certain conditions, the peak can slowly rotate even to a fixed external stimulus. The ring also exhibits hysteresis due to the subcritical nature of the bifurcation to sharp orientation tuning. Such behavior is shown to be consistent with a corresponding analog version of the IF model in the limit of slow synaptic interactions. For fast synapses, the deterministic fluctuations of the ISIs associated with the tuning curve can support a coefficient of variation of order unity.

1 Introduction

Recent studies of the formation of localized spatial patterns in one- and two-dimensional neural networks have been used to investigate a variety of neuronal processes including orientation selectivity in primary visual cortex (Ben-Yishai, Bar-Or, Lev, & Sompolinsky, 1995; Ben-Yishai, Hansel, & Sompolinsky, 1997; Hansel & Sompolinsky, 1997; Mundel, Dimitrov, & Cowan, 1997), the coding of arm movements in motor cortex (Lukashin & Georgopolous, 1994a, 1994b; Georgopolous, 1995), and the control of saccadic eye movements (Zhang, 1996). The networks considered in these studies are based on a simplified rate or analog model of a neuron, in which

the state of each neuron is characterized by a single continuous variable that determines its short-term average output activity (Cowan, 1968; Wilson & Cowan, 1972). All of these models involve the same basic dynamical mechanism for the formation of localized patterns: spontaneous symmetry breaking from a uniform resting state (Cowan, 1982). Localized structures consisting of a single peak of high activity occur when the maximum (spatial) Fourier component of the combination of excitatory and inhibitory interactions between neurons has a wavelength comparable to the size of the network. Typically such networks have periodic boundary conditions so that unraveling the network results in a spatially periodic pattern of activity, as studied previously by Ermentrout and Cowan (1979a, 1979b) (see also the review by Ermentrout, 1998).

In contrast to mean firing-rate models, there has been relatively little analytical work on pattern formation in more realistic spiking models. A number of numerical studies have shown that localized activity profiles can occur in networks of Hodgkin-Huxley neurons (Lukashin & Georgopolous, 1994a, 1994b; Hansel & Sompolinsky, 1996). Moreover, both local (Somers, Nelson, & Sur, 1995) and global (Usher, Stemmler, Koch, & Olami, 1994) patterns of activity have been found in integrate-and-fire (IF) networks. Recently a dynamical theory of global pattern formation in IF networks has been developed in terms of the nonlinear map of the neuronal firing times (Bressloff & Coombes, 1998b, 2000). A linear stability analysis of this map shows how, in the case of short-range excitation and long-range inhibition, a network that is synchronized in the weak coupling regime can destabilize as the strength of coupling is increased, leading to a state characterized by clustered but irregular fluctuations of the interspike intervals (ISIs). The separation of these clusters in phase-space results in a spatially periodic pattern of mean (time-averaged) firing rate across the network, which is modulated by deterministic fluctuations in the instantaneous firing rates.

In this article we apply the theory of Bressloff and Coombes (1998b, 2000) to the analysis of localized pattern formation in an IF version of the model of sharp orientation tuning developed by Hansel and Sompolinsky (1997) and Ben-Yishai et al. (1995, 1997). We first study a corresponding analog model in which the outputs of the neurons are taken to be mean firing rates. Since the resulting firing-rate function is nonlinear rather than semilinear, it is not possible to construct exact solutions for the orientation tuning curves along the lines of Hansel and Sompolinsky (1997). Instead, we investigate the existence and stability of such activity profiles using bifurcation theory. We show how a uniform resting state destabilizes to a stable localized pattern as the strength of neuronal recurrent interactions is increased. This localized state consists of a single narrow peak of activity whose center can lock to a slowly rotating, weakly tuned external stimulus. Interestingly, we find that the bifurcation from the resting state is subcritical: the system jumps to a localized activity profile on destabilization of the resting state, and

hysteresis occurs in the sense that sharp orientation tuning can coexist with a stable resting state.

We then turn to the full IF model and show how an analysis of the nonlinear firing time map can serve as a basis for understanding orientation tuning in networks of spiking neurons. We derive explicit criteria for the stability of phase-locked solutions by considering the propagation of perturbations of the firing times throughout the network. Our analysis identifies regions in parameter space where instabilities in the firing times cause (subcritical) bifurcations to non-phase-locked states that support localized patterns of mean firing rates across the network similar to the sharp orientation tuning curves found in the corresponding analog model. However, as found in the case of global pattern formation (Bressloff & Coombes, 1998b, 2000), the tuning curves are modulated by deterministic fluctuations of the ISIs on closed quasiperiodic orbits, which grow with the speed of synapses. For sufficiently fast synapses, the resulting coefficient of variation (C_V) can be of order unity and the ISIs appear to exhibit chaotic motion due to breakup of the quasiperiodic orbits.

2 The Model

We consider an IF version of the neural network model for orientation tuning in a cortical hypercolumn developed by Hansel and Sompolinsky (1997) and Ben-Yishai et al. (1997). This is a simplified version of the model studied numerically by Somers et al. (1995). The network consists of two subpopulations of neurons, one excitatory and the other inhibitory, which code for the orientation of a visual stimulus appearing in a common visual field (see Figure 1). The index $L = E, I$ will be used to distinguish the two populations. Each neuron is parameterized by an angle ϕ, $0 \leq \phi < \pi$, which represents its orientation preference. (The angle is restricted to be from 0 to π since a bar that is oriented at an angle 0 is indistinguishable from one that has an orientation π.) Let $U_L(\phi, t)$ denote the membrane potential at time t of a neuron of type L and orientation preference ϕ. The neurons are modeled as IF oscillators evolving according to the set of equations

$$\tau_0 \frac{\partial U_L(\phi, t)}{\partial t} = h_0 - U_L(\phi, t) + X_L(\phi, t), \qquad L = E, I, \qquad (2.1)$$

where h_0 is a constant external input or bias, τ_0 is a membrane time constant, and $X_L(\phi, t)$ denotes the total synaptic input to a neuron ϕ of type L. Periodic boundary conditions are assumed so that $U_L(0, t) = U_L(\pi, t)$. Equation 2.1 is supplemented by the condition that whenever a neuron reaches a threshold κ, it fires a spike, and its membrane potential is immediately reset to zero. In other words,

$$U_L(\phi, t^+) = 0 \quad \text{whenever} \quad U_L(\phi, t) = \kappa, \qquad L = E, I. \qquad (2.2)$$
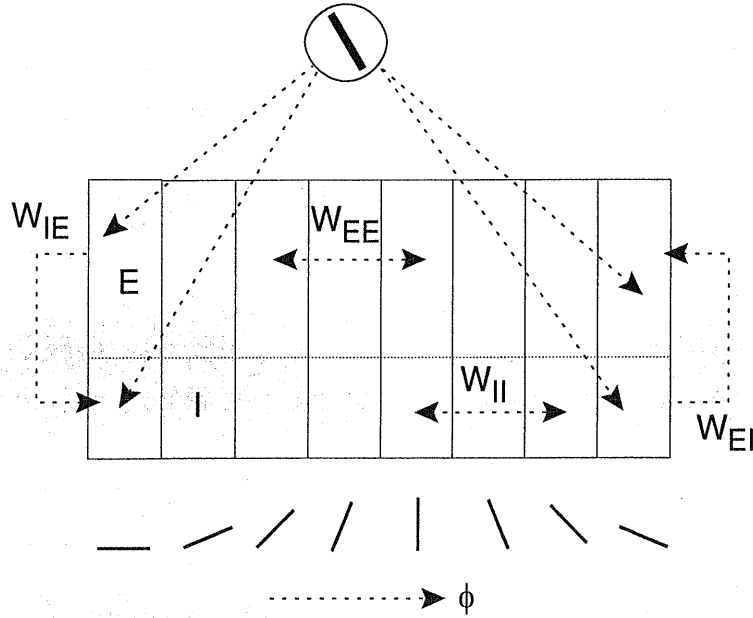
Figure 1: Network architecture of a ring model of a cortical hypercolumn (see Hansel & Sompolinsky, 1997).

For concreteness, we set the threshold $\kappa = 1$ and take $h_0 = 0.9 < \kappa$, so that in the absence of any synaptic inputs, all neurons are quiescent. We also fix the fundamental unit of time to be of the order 5–10 msec by setting $\tau_0 = 1$. (All results concerning firing rates or interspike intervals presented in this article are in units of τ_0.)

The total synaptic input $X_L(\phi, t)$ is taken to be of the form

$$X_L(\phi, t) = \sum_{M=E,I} \int_0^\pi \frac{d\phi'}{\pi} W_{LM}(\phi - \phi') Y_M(\phi', t) + h_L(\phi, t), \qquad (2.3)$$

where $W_{LM}(\phi - \phi')$ denotes the interaction between a presynaptic neuron ϕ' of type M and a postsynaptic neuron ϕ of type L, and $Y_M(\phi', t)$ is the effective input at time t induced by the incoming spike train from the presynaptic neuron (also known as the synaptic drive; Pinto, Brumberg, Simons, & Ermentrout, 1996). The term $h_L(\phi, t)$ represents the inputs from the lateral geniculate nucleus (LGN). The weight functions W_{LM} are taken to be even

and π-periodic in ϕ so that they have the Fourier expansions

$$W_{LE}(\phi) = W_0^{LE} + 2\sum_{k=1}^{\infty} W_k^{LE} \cos(2k\phi) \geq 0 \tag{2.4}$$

$$W_{LI}(\phi) = -W_0^{LI} - 2\sum_{k=1}^{\infty} W_k^{LI} \cos(2k\phi) \leq 0. \tag{2.5}$$

Moreover, the interactions are assumed to depend on the degree of similarity of the presynaptic and postsynaptic orientation preferences, and to be of maximum strength when they have the same preference. In order to make a direct comparison with the results of Hansel and Sompolinsky (1997), almost all our numerical results will include only the first two harmonics in equations 2.4 and 2.5. Higher harmonics (W_n^{LM}, $n \geq 2$) generate similar-looking tuning curves.

Finally, we take

$$Y_L(\phi, t) = \int_0^{\infty} d\tau \rho(\tau) f_L(\phi, t - \tau), \tag{2.6}$$

where $\rho(\tau)$ represents some delay distribution and $f_L(\phi, t)$ is the output spike train of a neuron ϕ of type L. Neglecting the pulse shape of an individual action potential, we represent the output spike train as a sequence of impulses,

$$f_L(\phi, t) = \sum_{k \in \mathbb{Z}} \delta(t - T_L^k(\phi)), \tag{2.7}$$

where $T_L^k(\phi)$, integer k, denotes the kth firing time (threshold-crossing time) of the given neuron. The delay distribution $\rho(\tau)$ can incorporate a number of possible sources of delay in neural systems: (1) discrete delays arising from finite axonal transmission times, (2) synaptic processing delays associated with the conversion of an incoming spike to a postsynaptic potential, or (3) dendritic processing delays in which the effects of a postsynaptic potential generated at a synapse located on the dendritic tree at some distance from the soma are mediated by diffusion along the tree. For concreteness, we shall restrict ourselves to synaptic delays and take $\rho(t)$ to be an alpha function (Jack, Noble, & Tsien, 1975; Destexhe, Mainen, & Sejnowsky, 1994),

$$\rho(\tau) = \alpha^2 \tau e^{-\alpha \tau} \Theta(\tau), \tag{2.8}$$

where α is the inverse rise time of a postsynaptic potential, and $\Theta(\tau) = 1$ if $\tau \geq 0$ and is zero otherwise. We expect axonal delays to be small within a given hypercolumn. (For a review of the dynamical effects of dendritic structure, see Bressloff & Coombes, 1997.)

It is important to see how the above spiking version of the ring model is related to the rate models considered by Hansel and Sompolinsky (1997) and Ben-Yishai et al. (1997). Suppose the synaptic interactions are sufficiently slow that the output $f_L(\phi, t)$ of a neuron can be characterized reasonably well by a mean (time-averaged) firing rate (see, for example, Amit & Tsodyks, 1991; Bressloff & Coombes, 2000). Let us consider the case in which $\rho(\tau)$ is given by the alpha function 2.8 with a synaptic rise time α^{-1} significantly longer than all other timescales in the system. The total synaptic input to neuron ϕ of type L will then be described by a slowly time-varying function $X_L(\phi, t)$, such that the actual firing rate will quickly relax to approximately the steady-state value, as determined by equations 2.1 and 2.2. This implies that

$$f_L(\phi, t) = f(X_L(\phi, t)),$$
(2.9)

with the steady-state firing-rate function f given by

$$f(X) = \left\{ \ln\left[\frac{h_0 + X}{h_0 + X - 1}\right] \right\}^{-1} \Theta(h_0 + X - 1).$$
(2.10)

(For simplicity, we shall ignore the effects of refractory period, which is reasonable when the system is operating well below its maximal firing rate.) Equation 2.9 relates the dynamics of the firing rate directly to the stimulus dynamics $X_L(\phi, t)$ through the steady-state response function. In effect, the use of a slowly varying distribution $\rho(\tau)$ allows a consistent definition of the firing rate so that a dynamical network model can be based on the steady-state properties of an isolated neuron.

Substitution of equations 2.6 and 2.9 into 2.3 yields the extended Wilson-Cowan equations (Wilson & Cowan, 1973):

$$X_L(\phi, t) = \sum_{M=E,I} \int_0^\pi \frac{d\phi'}{\pi} W_{LM}(\phi - \phi') \int_0^\infty d\tau \rho(\tau) f(X_M(\phi', t - \tau))$$

$$+ h_L(\phi, t).$$
(2.11)

An alternative version of equation 2.11 may be obtained for the alpha function delay distribution, 2.8, by rewriting equation 2.6 as the differential equation

$$\frac{1}{\alpha^2}\frac{\partial^2 Y_L}{\partial t^2} + \frac{2}{\alpha}\frac{\partial Y_L}{\partial t} + Y_L = f(X_L),$$
(2.12)

with X_L given by equation 2.3 and $Y_L(\phi, t), \partial Y_L(\phi, t)/\partial t \to 0$ as $t \to -\infty$. Similarly, taking $\rho(t) = \alpha e^{-\alpha t}$ generates the particular version of the Wilson-Cowan equations studied by Hansel and Sompolinsky (1997),

$$\alpha^{-1}\frac{\partial Y_L}{\partial t} + Y_L = f(X_L).$$
(2.13)

There are a number of differences, however, between the interpretation of Y_L in equation 2.13 and the corresponding variable considered by Hansel and Sompolinsky (1997). In the former case, $Y_L(\phi, t)$ is the synaptic drive of a single neuron with orientation preference ϕ, and f is a time-averaged firing rate, whereas in the latter case, Y_L represents the activity of a population of neurons forming an orientation column ϕ, and f is some gain function. It is possible to introduce the notion of an orientation column in our model by partitioning the domain $0 \leq \phi < \pi$ into N segments of length π/N such that

$$m_L(\phi_k, t) = N \int_{k\pi/N}^{(k+1)\pi/N} \frac{d\phi}{\pi} f_L(\phi, t), \qquad k = 0, 1, \ldots, N-1 \qquad (2.14)$$

represents the population-averaged firing rate within the kth orientation column, $\phi_k = k\pi/N$. (Alternatively, we could reinterpret the IF model as a caricature of a synchronized column of spiking neurons.)

Hansel and Sompolinsky (1997) and Ben-Yishai et al. (1995, 1997) have carried out a detailed investigation of orientation tuning in the mean firing-rate version of the ring model defined by equations 2.3 and 2.13 with f a semilinear gain function. They consider external inputs of the form

$$h_L(\phi, t) = C\Gamma_L[1 - \chi + \chi \cos(2(\phi - \phi_0(t)))] \qquad (2.15)$$

for $0 \leq \chi \leq 0.5$. This represents a tuned input from the LGN due to a visual stimulus of orientation ϕ_0. The parameter C denotes the contrast of the stimulus, Γ_L is the transfer function from the LGN to the cortex, and χ determines the angular anisotropy. In the case of a semilinear gain function, $f(x) = 0$ if $x \leq 0$, $f(x) = x$ if $x \geq 0$, and $f(x) = 1$ for $x \geq 1$, it is possible to derive self-consistency equations for the activity profile of the network. Solving these equations shows that in certain parameter regimes, local cortical feedback can generate sharp orientation tuning curves in which only a fraction of neurons are active. The associated activity profile consists of a single peak centered about ϕ_0 (Hansel & Sompolinsky, 1997). This activity peak can also lock to a rotating stimulus $\phi_0 = \Omega t$ provided that Ω is not too large; if the inhibitory feedback is sufficiently strong, then it is possible for spontaneous wave propagation to occur even in the absence of a rotating stimulus (Ben-Yishai et al., 1997).

The idea that local cortical interactions play a central role in generating sharp orientation tuning curves is still controversial. The classical model of Hubel and Wiesel (1962) proposes a very different mechanism, in which the orientation preference of a cell arises primarily from the geometrical alignment of the receptive fields of the LGN neurons projecting to it. A number of recent experiments show a significant correlation between the alignment of receptive fields of LGN neurons and the orientation preference of simple cells functionally connected to them (Chapman, Zahs, &

Stryker, 1991; Reid & Alonso, 1995). In addition, Ferster, Chung, and Wheat
(1997) have shown that cooling a patch of cortex and therefore presumably
abolishing cortical feedback does not totally abolish the orientation tuning
exhibited by excitatory postsynaptic potentials (EPSPs) generated by LGN
input. However, there is also growing experimental evidence suggesting
the importance of cortical feedback. For example, the blockage of extracel-
lular inhibition in cortex leads to considerably less sharp orientation tuning
(Sillito, Kemp, Milson, & Beradi, 1980; Ferster & Koch, 1987; Nelson, Toth,
Seth, & Mur, 1994). Moreover, intracellular measurements indicate that di-
rect inputs from the LGN to neurons in layer 4 of the primary visual cortex
provide only a fraction of the total excitatory inputs relevant to orientation
selectivity (Pei, Vidyasagar, Volgushev, & Creutzseldt, 1994; Douglas, Koch,
Mahowald, Martin, & Suarez, 1995; see also Somers et al., 1995). In addition,
there is evidence that orientation tuning takes about 50 to 60 msec to reach
its peak, and that the dynamics of tuning has a rather complex time course
(Ringach, Hawken, & Shapley, 1997), suggesting some cortical involvement.

The dynamical mechanism for sharp orientation tuning identified by
Hansel and Sompolinsky (1997) can be interpreted as a localized form of
spontaneous pattern formation (at least for strongly modulated cortical in-
teractions). For general spatially distributed systems, pattern formation con-
cerns the loss of stability of a spatially uniform state through a bifurcation
to a spatially periodic state (Murray, 1990). The latter may be stationary or
oscillatory (time periodic). Pattern formation in neural networks was first
studied in detail by Ermentrout and Cowan (1979a, 1979b). They showed
how competition between short-range excitation and long-range inhibition
in a two-dimensional Wilson-Cowan network can induce periodic striped
and hexagonal patterns of activity. These spontaneous patterns provided a
possible explanation for the generation of visual hallucinations. (See also
Cowan, 1982.) At first sight, the analysis of orientation tuning by Hansel and
Sompolinsky (1997) and Ben-Yishai et al. (1997) appears to involve a differ-
ent dynamical mechanism from this, since only a single peak of activity is
formed over the domain $0 \leq \phi \leq \pi$ rather than a spatially repeating pattern.
This apparent difference vanishes, however, once it is realized that spatially
periodic patterns would be generated by "unraveling" the ring. Thus, the
one-dimensional stationary and propagating activity profiles that Wilson
and Cowan (1973) found correspond, respectively, to stationary and time-
periodic patterns on the π periodic ring. In the following sections, we study
orientation tuning in both the analog and IF models from the viewpoint of
spontaneous pattern formation.

3 Orientation Tuning in Analog Model

We first consider orientation tuning in the analog or rate model described
by equation 2.11 with the firing-rate function given by equation 2.10. This
may be viewed as the $\alpha \to 0$ limit of the IF model. We shall initially restrict

ourselves to the case of time-independent external inputs $h_L(\phi)$. Given a ϕ-independent input $h_L(\phi) = C_L$, the homogeneous equation 2.11 has at least one spatially uniform solution $X_L(\phi, t) = \overline{X}_L$, where

$$\overline{X}_L = \sum_{M=E,I} W_0^{LM} f(\overline{X}_M) + C_L. \tag{3.1}$$

The local stability of the homogeneous state is found by linearizing equation 2.11 about $\overline{X}_L$. Setting $x_L(\phi, t) = X_L(\phi, t) - \overline{X}_L$ and expanding to first order in x_L gives

$$x_L(\phi, t) = \sum_{M=E,I} \gamma_M \int_0^\pi \frac{d\phi'}{\pi} W_{LM}(\phi - \phi') \int_0^\infty d\tau \rho(\tau) x_M(\phi', t - \tau), \tag{3.2}$$

where $\gamma_M = f'(\overline{X}_M)$ and $f' \equiv df/dX$. Equation 3.2 has solutions of the form

$$x_L(\phi, t) = Z_L e^{\nu t} e^{\pm 2in\phi}. \tag{3.3}$$

For each n, the eigenvalues ν and corresponding eigenvectors $\mathbf{Z} = (Z_E, Z_I)^{\text{tr}}$ satisfy the equation

$$\mathbf{Z} = \widetilde{\rho}(\nu) \widehat{\mathbf{W}}_n \mathbf{Z}, \tag{3.4}$$

where

$$\widetilde{\rho}(\nu) \equiv \int_0^\infty e^{-\nu\tau} \rho(\tau) d\tau = \frac{\alpha^2}{(\alpha + \nu)^2} \tag{3.5}$$

for the alpha function 2.8, and

$$\widehat{\mathbf{W}}_n = \begin{pmatrix} \gamma_E W_n^{EE} & -\gamma_I W_n^{EI} \\ \gamma_E W_n^{IE} & -\gamma_I W_n^{II} \end{pmatrix}. \tag{3.6}$$

The state $\overline{X}_L$ will be stable if all eigenvalues ν have a negative real part. It follows that the stability of the homogeneous state depends on the particular choice of weight parameters W_n^{LM} and the external inputs C_L, which determine the factors γ_L. On the other hand, stability is independent of the inverse rise time α. (This α independence will no longer hold for the IF model; see section 4.)

In order to simplify matters further, let us consider a symmetric two-population model in which

$$C_L = C, \qquad W_n^{EE} = W_n^{IE} \equiv W_n^E, \qquad W_n^{EI} = W_n^{II} \equiv W_n^I. \tag{3.7}$$

Equation 3.1 then has a solution $X_L = \overline{X}$, where $\overline{X}$ is the unique solution of the equation $\overline{X} = W_0 f(\overline{X}) + C$. We shall assume that C is superthreshold, $h_0 + C > 1$; otherwise $\overline{X} = C$ such that $f(\overline{X}) = 0$. Moreover, $\gamma_L = \gamma \equiv f'(\overline{X})$ for $L = E, I$ so that $\widehat{W}_n = \gamma W_n$. Equations 3.4 through 3.6 then reduce to the eigenvalue equation

$$\left(\frac{\nu}{\alpha} + 1\right)^2 = \gamma \lambda_n^{\pm} \tag{3.8}$$

for integer n, where $\lambda_n^{\pm}$ are the eigenvalues of the weight matrix W_n with corresponding eigenvectors $Z_n^{\pm}$:

$$\lambda_n^+ = W_n \equiv W_n^E - W_n^I, \quad \lambda_n^- = 0, \quad Z_n^+ = \begin{pmatrix} 1 \\ 1 \end{pmatrix}, \quad Z_n^- = \begin{pmatrix} 1/W_n^E \\ 1/W_n^I \end{pmatrix}. \tag{3.9}$$

It follows from equation 3.8 that $\overline{X}$ is stable with respect to excitation of the $(-)$ modes $Z_0^-, Z_n^- \cos(2k\phi), Z_n^- \sin(2k\phi)$. If $\gamma W_n < 1$ for all n then $\overline{X}$ is also stable with respect to excitation of the corresponding $(+)$ modes. This implies that the effect of the superthreshold LGN input $h_L(\phi) = C$ is to switch the network from an inactive state to a stable homogeneous active state. In this parameter regime, sharp orientation tuning curves can be generated only if there is a sufficient degree of angular anisotropy in the afferent inputs to the cortex from the LGN, that is, χ in equation 2.15 must be sufficiently large (Hansel & Sompolinsky, 1997). This is the classical model of orientation tuning (Hubel & Wiesel, 1962).

An alternative mechanism for sharp orientation tuning can be obtained by having strongly modulated cortical interactions such that $\gamma W_n < 1$ for all $n \neq 1$ and $\gamma W_1 > 1$. The homogeneous state then destabilizes due to excitation of the first harmonic modes $Z_1^+ \cos(2\phi), Z_1^+ \sin(2\phi)$. Since these modes have a single maximum in the interval $(0, \pi)$, we expect the network to support an activity profile consisting of a solitary peak centered about some angle ϕ_0, which is the same for both the excitatory and inhibitory populations. For ϕ-independent external inputs ($\chi = 0$), the location of this center is arbitrary, which reflects the underlying translational invariance of the network. Following Hansel and Sompolinsky (1997), we call such an activity profile a marginal state. The presence of a small, angular anisotropy in the inputs ($0 < \chi \ll 1$ in equation 2.15) breaks the translational invariance of the system and locks the location of the center to the orientation corresponding to the peak of the stimulus (Hansel & Sompolinsky, 1997; Ben-Yishai et al., 1997). In contrast to afferent mechanisms of sharp orientation tuning, χ can be arbitrarily small.

From the symmetries imposed by equations 3.7, we can restrict ourselves to the class of solutions $X_L(t) = X(t)$, $L = E, I$, such that equation 2.11 reduces to the effective one-population model

$$X(\phi, t) = \int_0^\pi \frac{d\phi'}{\pi} W(\phi - \phi') \int_0^\infty d\tau \rho(\tau) f(X(\phi', t - \tau)) + C, \tag{3.10}$$
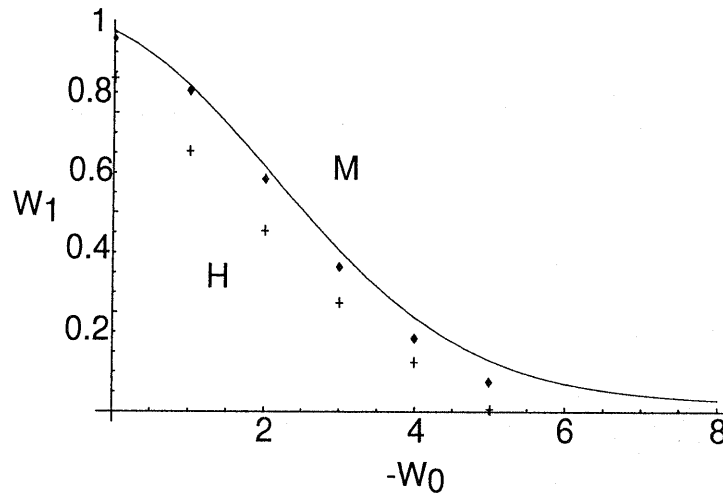
Figure 2: Phase boundary in the (W_0, W_1)-plane (solid curve) between a stable homogeneous state (H) and a stable marginal state (M) of the analog model for $C = 1$. Also shown are data points from a direct numerical simulation of a symmetric two-population network consisting of $N = 100$ neurons per population and sinusoidal-like weight kernel $W(\phi) = W_0 + 2W_1 \cos(2\phi)$. (a) Critical coupling for destabilization of homogeneous state (solid diamonds). (b) Lower critical coupling for persistence of stable marginal state due to hysteresis (crosses).

with $W(\phi) = W_0 + 2\sum_{n=1}^{\infty} W_n \cos(2n\phi)$ and W_n fixed such that $\gamma W_n < 1$ for all $n \neq 1$. Treating W_1 as a bifurcation parameter, the critical coupling at which the marginal state becomes excited is given by $W_1 = W_{1c}$, where $W_{1c} = 1/f'(\overline{X})$ with $\overline{X}$ dependent on W_0 and C. This generates a phase boundary curve in the (W_0, W_1)-plane that separates a stable homogeneous state and a marginal state. (See the solid curve in Figure 2.) When the phase boundary is crossed from below, the network jumps to a stable marginal state consisting of a sharp orientation tuning curve whose width (equal to $\pi/2$) is invariant across the parameter domain over which it exists. This reflects the fact that the underlying pattern-forming mechanism selects out the first harmonic modes. On the other hand, the height and shape of the tuning curve will depend on the particular choice of weight coefficients W_n as well as other parameters, such as the contrast C. Note that sufficiently far from the bifurcation point, additional harmonic modes will be excited, which may modify the width of the tuning curve, leading to a dependence on the weights W_n. Indeed, in the case of a semilinear firing-rate function, the width of the sharp tuning curve is found to be dependent on the weights W_n (Hansel & Sompolinsky, 1997), reflect-

ing the absence of an additional nonlinearity selecting out the fundamental harmonic.

Examples of typical tuning curves are illustrated in Figure 3a, where we show results of a direct numerical simulation of a symmetric two-population analog network. The steady-state firing rate $f(\phi)$ of the marginal state is plotted as a function of orientation preference ϕ in the case of a cosine weight kernel $W(\phi) = W_0 + 2W_1 \cos(2\phi)$. It can be seen that the height of the activity profile increases with the weight W_1. Note, however, that if W_1 becomes too large, then the marginal state is itself destroyed by amplitude instabilities. The height also increases with contrast C. Consistent with the results of Hansel and Sompolinsky (1997) and Ben-Yishai et al. (1997), the center of the activity peak can lock to a slowly rotating, weakly tuned stimulus as illustrated in Figure 3b. Also shown in Figure 3a is the tuning curve for a Mexican hat weight kernel $W(\phi) = A_1 e^{-\phi^2/2\sigma_1^2} - A_2 e^{-\phi^2/2\sigma_2^2}$ over the range $-\pi/2 \le \phi \le \pi/2$. The constants σ_i, A_i are chosen so that the corresponding Fourier coefficients satisfy $\gamma W_1 > 1$ and $\gamma W_n < 1$ for all $n \ne 1$. The shape of the tuning curve is very similar to that obtained using the simple cosine. To reproduce more closely biological tuning curves, which have a sharper peak and broader shoulders than obtained here, it is necessary to introduce some noise into the system (Dimitrov & Cowan, 1998). This smooths the firing rate function, 2.10, to yield a sigmoid-like nonlinearity.

Interestingly, the marginal state is found to exhibit hysteresis in the sense that sharp orientation tuning persists for a range of values of $W_1 < W_{1c}$. That is, over a certain parameter regime, a stable homogeneous state and a stable marginal state coexist (see data points in Figure 2). This suggests that the bifurcation is subcritical, which is indeed found to be the case, as we now explain. In standard treatments of pattern formation, bifurcation theory is used to derive nonlinear ordinary differential equations for the amplitude of the excited modes from which existence and stability can be determined, at least close to the bifurcation point (Cross & Hohenberg, 1993; Ermentrout, 1998). Suppose that the firing-rate function f is expanded about the (nonzero) fixed point $\overline{X}$,

$$f(X) - f(\overline{X}) = \gamma(X - \overline{X}) + g_2(X - \overline{X})^2 + g_3(X - \overline{X})^3 + \cdots, \qquad (3.11)$$

where $\gamma = f'(\overline{X})$, $g_2 = f''(\overline{X})/2$, $g_3 = f'''(\overline{X})/6$. Introduce the small parameter ϵ according to $W_1 - W_{1c} = \epsilon^2$ and substitute into equation 3.10 the perturbation expansion,

$$X(\phi, t) - \overline{X} = \left[Z(t)e^{2in\phi} + Z^*(t)e^{-2in\phi} \right] + \mathcal{O}(\epsilon^2), \qquad (3.12)$$

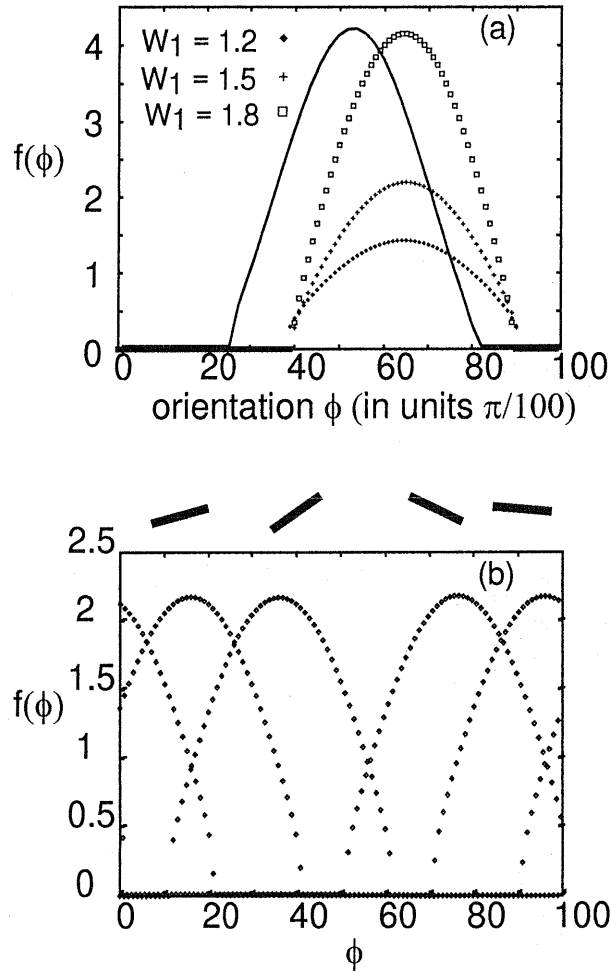where $Z(t)$, $Z^*(t)$ denote a complex conjugate pair of $\mathcal{O}(\epsilon)$ amplitudes.

Figure 3: Sharp orientation tuning curves for a symmetric two-population analog network ($N = 100$) with cosine weight kernel $W(\phi) = W_0 + 2W_1 \cos(2\phi)$. (a) The firing rate $f(\phi)$ is plotted as a function of orientation preference ϕ for various W_1 with $W_0 = -0.1$, $C = 0.25$ and $\alpha = 0.5$. Also shown (solid curve) is the corresponding tuning curve for a Mexican hat weight kernel with $\sigma_1 = 20$ degrees, $\sigma_2 = 60$ degrees, and $A_i = A/\sqrt{2\pi\sigma_i^2}$. (b) Locking of tuning curve to a slowly rotating, weakly tuned external stimulus. Here $W_0 = -0.1$, $W_1 = 1.5$, $C = 0.25$, $\alpha = 1.0$. The degree of angular anisotropy in the input is $\chi = 0.1$, and the angular frequency of rotation is $\Omega = 0.0017$ (which corresponds to approximately 10 degrees per second).

A standard perturbation calculation (see appendix A and Ermentrout, 1998) shows that $Z(t)$ evolves according to an equation of the form

$$\frac{dZ}{dt} = Z\left(W_1 - W_{1c} + A|Z|^2\right),$$ (3.13)

where

$$A = \frac{3g_3}{\gamma^2} + \frac{2g_2^2}{\gamma^2}\left[\frac{W_2}{1 - \gamma W_2} + \frac{2W_0}{1 - \gamma W_0}\right].$$ (3.14)

Since W_1 and A are all real, the phase of Z is arbitrary (reflecting a marginal state), whereas the amplitude is given by $|Z| = \sqrt{|W_1 - W_{1c}|/A}$. It is clear that a stable marginal state will bifurcate from the homogeneous state if and only if $A < 0$. A quick numerical calculation shows that $A > 0$ for all W_0, W_2, and C. This implies that the bifurcation is subcritical, that is, the resting state bifurcates to an unstable broadly tuned orientation curve whose amplitude is $\mathcal{O}(\epsilon)$. Since the bifurcating tuning curve is unstable, it is not observed in practice; rather, one finds that the system jumps to a stable, large-amplitude, sharp tuning curve that coexists with the resting state and leads to hysteresis effects as illustrated schematically in Figure 4a. Note that in the case of sigmoidal firing-rate functions $f(X)$, the bifurcation may be either sub- or supercritical, depending on the relative strengths of recurrent excitation and lateral inhibition (Ermentrout & Cowan, 1979b). If the latter is sufficiently strong, then supercritical bifurcations can occur in which the resting state changes smoothly into a sharply tuned state. However, in the case studied here, the nonlinear firing-rate function $f(X)$ of equation 2.10 is such that the bifurcation is almost always subcritical.

The underlying translational invariance of the network means that the center of the tuning curve remains undetermined for a ϕ-independent LGN input (marginal stability). The center can be selected by including a small degree of angular anisotropy along the lines of equation 2.15. Suppose, in particular, that we replace C on the right-hand side of equation 3.10 by an LGN input of the form $h(\phi, t) = C[1 - \chi + \chi \cos(2[\phi - \omega t])]$ for some slow frequency ω. If we take $\chi = \epsilon^3$, then the amplitude equation 3.13 becomes

$$\frac{dZ}{dt} = Z\left(W_1 - W_{1c} + A|Z|^2\right) + Ce^{-2i\omega t}.$$ (3.15)

Writing $Z = re^{-2i(\theta + \omega t)}$ (with the phase θ defined in a rotating frame), we obtain the pair of equations:

$$\dot{r} = r(W_1 - W_{1c} + Ar^2) + C\cos 2\theta$$ (3.16)

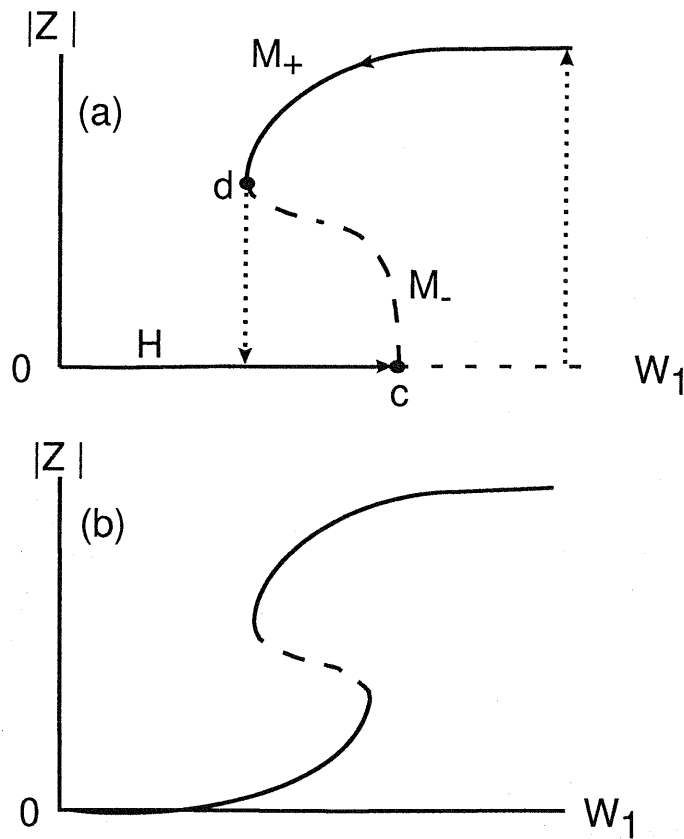$$\dot{\theta} = \omega - \frac{C}{2r}\sin(2\theta).$$ (3.17)

Figure 4: (a) Schematic diagram illustrating hysteresis effects in the analog model. As the coupling parameter W_1 is slowly increased from zero, a critical point c is reached where the homogeneous resting state (H) becomes unstable, and there is a subcritical bifurcation to an unstable, broadly tuned marginal state (M_-). Beyond the bifurcation point, the system jumps to a stable, sharply tuned marginal state (M_+), which coexists with the other solutions. If the coupling W_1 is now slowly reduced, the marginal state M_+ persists beyond the original point c so that there is a range of values $W_1(d) < W_1 < W_1(c)$ over which a stable resting state coexists with a stable marginal state (bistability). At point d, the states $M_\pm$ annihilate each other, and the system jumps back to the resting state. (b) Illustration of an imperfect bifurcation in the presence of a small degree of anisotropy in the LGN input. Thick solid (dashed) lines represent stable (unstable) states.

Thus, provided that ω is sufficiently small, equation 3.17 will have a stable fixed-point solution in which the phase ϕ of the pattern is entrained to the signal. Another interesting consequence of the anisotropy is that it generates an imperfect bifurcation for the (real) amplitude r due to the presence of the r-independent term $\delta = C\cos(2\theta)$ on the right-hand side of equation 3.16. This is illustrated in Figure 4b.

4 Orientation Tuning in IF Model

Our analysis of the analog model in section 3 ignored any details concerning neural spike trains by taking the output of a neuron to be an average firing rate. We now return to the more realistic IF model of equations 2.1 through 2.3 in which the firing times of individual spikes are specified. We wish to identify the analogous mechanism for orientation tuning in the model with spike coding.

4.1 Existence and Stability of Synchronous State.
The first step is to specify what is meant by a homogeneous activity state. We define a phase-locked solution to be one in which every oscillator resets or fires with the same collective period T that must be determined self-consistently. The state of each oscillator can then be characterized by a constant phase $\eta_L(\phi)$ with $0 \le \eta_L(\phi) < 1$ and $0 \le \phi < \pi$. The corresponding firing times satisfy $T_L^k(\phi) = (k - \eta_L(\phi))T$, integer k. Integrating equation 2.1 between two successive firing events and incorporating the reset condition 2.2 leads to the phase equations

$$1 = (1 - e^{-T})(h_0 + C_L)$$

$$+ \sum_{M=E,I} \int_0^\pi \frac{d\phi'}{\pi} W_{LM}(\phi - \phi')K_T(\eta_M(\phi') - \eta_L(\phi)), \quad L = E, I \quad (4.1)$$

where $W_{LM}(\phi)$ is given by equations 2.4 and 2.5, and

$$K_T(\eta) = e^{-T} \int_0^T dt\, e^t \sum_{k \in \mathbb{Z}} \rho(t + (k + \eta)T). \tag{4.2}$$

Note that for any phase-locked solution of equation 4.1, the distribution of network output activity across the network, as specified by the ISIs

$$\Delta_L^k(\phi) = T_L^{k+1}(\phi) - T_L^k(\phi), \tag{4.3}$$

is homogeneous since $\Delta_L^k(\phi) = T$ for all $k \in \mathbb{Z}$, $0 \le \phi < \pi$, $L = (E, I)$. In other words, each phase-locked state plays an analogous role to the homogeneous state $\overline{X}_L$ of the mean firing-rate model. To simplify our analysis, we shall concentrate on instabilities of the synchronous state $\eta_L(\phi) = \overline{\eta}$, where $\overline{\eta}$ is an arbitrary constant. In order to ensure such a solution exists, we impose
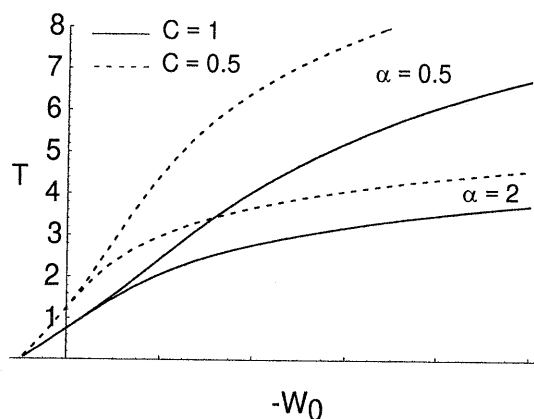
Figure 5: Variation of collective period T of synchronous state as a function of W_0 for different contrasts C and inverse rise times α.

the conditions 3.7 so that equation 4.1 reduces to a single self-consistency equation for the collective period T of the synchronous solution

$$1 = (1 - e^{-T})C_0 + W_0 K_T(0),\tag{4.4}$$

where we have set $C_0 = h_0 + C$ and $W_0 = W_0^E - W_0^I$. Solutions of equation 4.4 are plotted in Figure 5.

The linear stability of the synchronous state can be determined by considering perturbations of the firing times (van Vreeswijk, 1996; Gerstner, van Hemmen, & Cowan, 1996; Bressloff & Coombes, 1998a, 1998b, 2000):

$$T_L^k(\phi) = (k - \bar{\eta})T + \delta_L^k(\phi).\tag{4.5}$$

Integrating equation 2.1 between two successive firing events yields a nonlinear mapping for the firing times that can be expanded as a power series in the perturbations $\delta_L^k(\phi)$. This generates a linear difference equation of the form

$$A_T \left[\delta_L^{k+1}(\phi) - \delta_L^k(\phi) \right]$$

$$= \sum_{l=0}^{\infty} G_T(l) \int_0^\pi \frac{d\phi'}{\pi} \sum_{M=E,I} W_{LM}(\phi - \phi') \left[\delta_M^{k-l}(\phi') - \delta_L^k(\phi) \right]\tag{4.6}$$

with

$$G_T(l) = e^{-T} \int_0^T dt\, e^t \rho'(t + lT)\tag{4.7}$$

$$A_T = C_0 - 1 + W_0 \sum_{k \in \mathbb{Z}} \rho(kT). \tag{4.8}$$

Equation 4.6 has solutions of the form

$$\delta_L^k(\phi) = e^{k\nu} e^{\pm 2in\phi} \delta_L, \qquad L = E, I, \tag{4.9}$$

where $\nu \in \mathbb{C}$ and $0 \leq \text{Im } \nu < 2\pi$. The eigenvalues ν and associated eigenvectors $\mathbf{Z} = (\delta_E, \delta_I)^{\text{tr}}$ for each integer n satisfy the equation

$$A_T[e^\nu - 1]\mathbf{Z} = \left[\widetilde{G}_T(\nu)\mathbf{W}_n - \widetilde{G}_T(0)\mathbf{D} \right] \mathbf{Z}, \tag{4.10}$$

where

$$\widetilde{G}_T(\nu) = \sum_{k=0}^{\infty} G_T(k)e^{-k\nu} \tag{4.11}$$

and

$$\mathbf{W}_n = \begin{pmatrix} W_n^{EE} & -W_n^{EI} \\ W_n^{IE} & -W_n^{II} \end{pmatrix}, \qquad \mathbf{D} = \begin{pmatrix} W_0^{EE} - W_0^{EI} & 0 \\ 0 & W_0^{IE} - W_0^{II} \end{pmatrix}. \tag{4.12}$$

In order to simplify the subsequent analysis, we impose the same symmetry conditions 3.7 as used in the study of the analog model in section 3. We can then diagonalize equation 4.10 to obtain the result

$$A_T[e^\nu - 1] = \widetilde{G}_T(\nu)\lambda_n^\pm - \widetilde{G}_T(0)W_0, \tag{4.13}$$

where $\lambda_n^\pm$ are the eigenvalues of the weight matrix $\mathbf{W}_n$ (see equation 3.9). Note that one solution of equation 4.13 is $\nu = 0$ and $n = 0$ associated with excitation of the uniform (+) mode. This reflects invariance of the system with respect to uniform phase shifts in the firing times. The synchronous state will be stable if all other solutions of equation 4.13 satisfy Re $\nu < 0$. Following Bressloff and Coombes (2000), we investigate stability by first looking at the weak coupling regime in which $W_n = \mathcal{O}(\epsilon)$ for some $\epsilon \ll 1$. Performing a perturbation expansion in ϵ, it can be established that the stability of the synchronous state is determined by the nonzero eigenvalues in a small neighborhood of the origin, and these satisfy the equation (to first order in ϵ) $A_T\nu = (\lambda_n^\pm - W_0)\widetilde{G}_T(0)$. For the alpha function 2.8, it can be established that $A_T > 0$, whereas $\widetilde{G}_T(0) \equiv K_T'(0)/T < 0$. Therefore, the synchronous state is stable in the weak coupling regime provided that $W_n > W_0$ for all $n \neq 0$ and $W_0 < 0$. Assuming that these two conditions are satisfied, we now investigate what happens as the strength of coupling W_1 is increased for fixed W_n, $n \neq 1$. First, it is easy to establish that the

synchronous state cannot destabilize due to a real eigenvalue ν crossing the origin. In particular, it is stable with respect to excitations of the (−) modes. Thus, any instability will involve one or more complex conjugate pairs of eigenvalues $\nu = \pm i\omega$ crossing the imaginary axis, signaling (for $\omega \neq \pi$) the onset of a discrete Hopf bifurcation (or Neimark-Sacker bifurcation) of the firing times due to excitation of a (+) mode $\delta_L^k(\phi) = e^{\pm i\omega_0 k} e^{\pm i2\phi}$, $L = E, I$. In the special case $\omega = \pi$, this reduces to a subharmonic or period doubling bifurcation since $e^{\pm i\pi} = -1$.

4.2 Desynchronization Leading to Sharp Orientation Tuning. In order to investigate the occurrence of a Hopf (or period-doubling) bifurcation in the firing times, substitute $\nu = i\omega$ into equation 4.13 for $n = 1$ with $\lambda_1^+ = W_1$ and equate real and imaginary parts to obtain the pair of equations

$$A_T[\cos(\omega) - 1] = W_1 \widetilde{C}(\omega) - W_0 \widetilde{C}(0), \quad A_T \sin(\omega) = -W_1 \widetilde{S}(\omega), \quad (4.14)$$

where

$$\widetilde{C}(\omega) = \text{Re } \widetilde{G}_T(i\omega), \quad \widetilde{S}(\omega) = -\text{Im } \widetilde{G}_T(i\omega). \quad (4.15)$$

Explicit expressions for $\widetilde{C}(\omega)$ and $\widetilde{S}(\omega)$ in the case of the alpha function delay distribution 2.8 are given in appendix B. Suppose that α, W_0, and C_0 are fixed, with $T = T(\alpha, W_0, C_0)$ the unique self-consistent solution of equation 4.4 (see Figure 5). The smallest value of the coupling parameter, $W_1 = W_{1c}$, for which a nonzero solution, $\omega = \omega_0 \neq 0$, of the simultaneous equations 4.14 is then sought. This generates a phase boundary curve in the (W_0, W_1) plane, as illustrated in Figure 6 for various C and α. Phase boundaries in the (α, W_1) plane and the (C, W_1) plane are shown in Figures 7 and 8, respectively.

The cusps of the boundary curves in these figures correspond to points where two separate solution branches of equation 4.14 cross; only the lower branch is shown since this determines the critical coupling for destabilization of the synchronous state. The region below a given boundary curve includes the origin. Weak coupling theory shows that in a neighborhood of the origin, the synchronous state is stable. Therefore, the boundary curve is a locus of bifurcation points separating a stable homogeneous state from a marginal non-phase-locked state. It should also be noted that for each boundary curve in Figures 6 and 7, the left-hand branch signals the onset of a (subcritical) Hopf bifurcation ($\omega_0 \neq \pi$), whereas the right-hand branch signals the onset of a (subcritical) period doubling bifurcation ($\omega_0 = \pi$); the opposite holds true in Figure 8. However, there is no qualitative difference in the observed behavior induced by these two types of instability.

Direct numerical simulations confirm that when a phase boundary curve is crossed from below, the IF network jumps to a stable marginal state consisting of a sharp orientation tuning curve as determined by the spatial
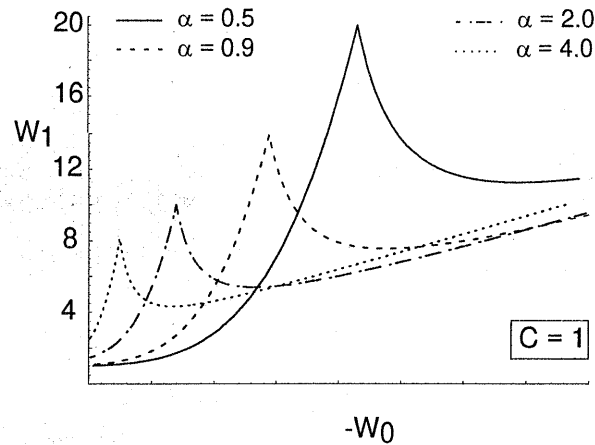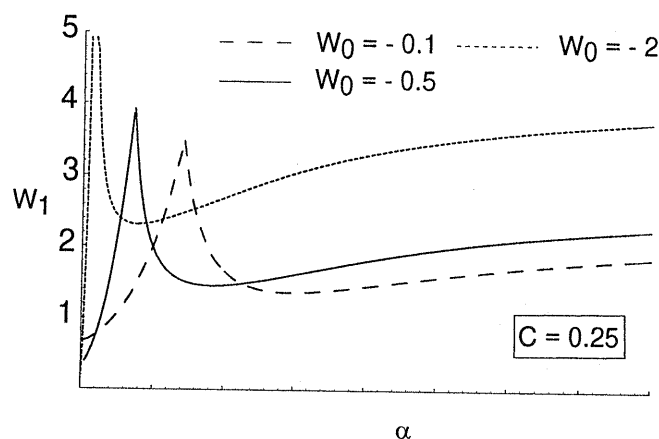
Figure 6: Phase boundary in the (W_0, W_1) plane between a stable synchronous state and a marginal state of a symmetric two-population IF network. Boundary curves are shown for $C = 1$ and various values of the inverse rise time α. In each case, the synchronous state is stable below a given boundary curve.

distribution of the mean (time-averaged) firing rates $a(\phi)$. The latter are defined according to $a(\phi) = \overline{\Delta}(\phi)^{-1}$ where

$$\overline{\Delta}(\phi) = \lim_{M \to \infty} \frac{1}{2M+1} \sum_{m=-M}^{M} \Delta^m(\phi), \qquad (4.16)$$

with $\Delta^m(\phi)$ given by equation 4.3. (We do not distinguish between excitatory and inhibitory neurons here since they behave identically in a symmetric two-population network.) The resulting long-term average behavior of the IF network for $W_1 > W_{1c}$ is illustrated in Figure 9a. For the given choice of parameter values, the activity profile is in good quantitative agreement with the corresponding profile obtained in the analog version of the network (see Figure 3). Moreover, as in the case of the analog network, (1) the marginal state exhibits hysteresis (suggesting that the bifurcation is subcritical), and (2) the center of the sharp orientation tuning curve is able to lock to a slowly rotating, weakly tuned external stimulus (see Figure 9b).

Comparison of the phase diagrams of the IF model (Figures 6–8) and the corresponding analog model (Figure 2) shows a major difference in the predicted value of the critical coupling W_{1c} in the two models. The critical coupling W_{1c} in the IF model converges to the corresponding analog result (which is α-independent) in the limit $\alpha \to 0$. This is particularly clear in Figure 8. However, for nonzero α, we expect good quantitative

Figure 7: Phase boundary in the (α, W_1) plane between a stable homogeneous state and a marginal state of a symmetric two-population IF network. Boundary curves are shown for $C = 0.25$ and various values of W_0.

agreement between the two models only when (1) there is an approximate balance between the mean excitatory and inhibitory coupling ($W_0 \approx 0$) and (2) synaptic interactions are sufficiently slow ($\alpha \ll 1$). Both conditions hold in Figures 9. Outside this parameter regime, the higher value of W_{1c} for the IF model leads to relatively high levels of mean firing rates in the activity profile of the marginal state, since large values of W_1 imply strong short-range excitation. The condition $W_0 \approx 0$ can be understood in terms of the self-consistency condition for the collective period T of the synchronous state given by equation 4.4. As W_0 becomes more negative, the period T increases (see Figure 5) so that $\alpha T > 1$ and the reduction to the analog model is no longer a good approximation. (In Bressloff & Coombes, 2000, the period T is kept fixed by varying the external input.)

4.3 Quasiperiodicity and Interspike Interval Variability. We now explore in more detail the nature of the spatiotemporal dynamics of the ISIs occurring in the marginal state of the IF model. For concreteness, we consider a symmetric two-population network with $W_n = 0$ for all $n \geq 2$. We shall proceed by fixing the parameters W_0, W_1, and C such that a sharp orientation tuning curve exists and considering what happens as α is increased. In Figure 10 we plot the ISI pairs $(\Delta^{n-1}(\phi), \Delta^n(\phi))$, integer n, for all the excitatory neurons in the ring. It can be seen from Figure 10a that for relatively slow synapses ($\alpha = 2$), the temporal fluctuations in the ISIs are negligible. There exists a set of spatially separated points reflecting the
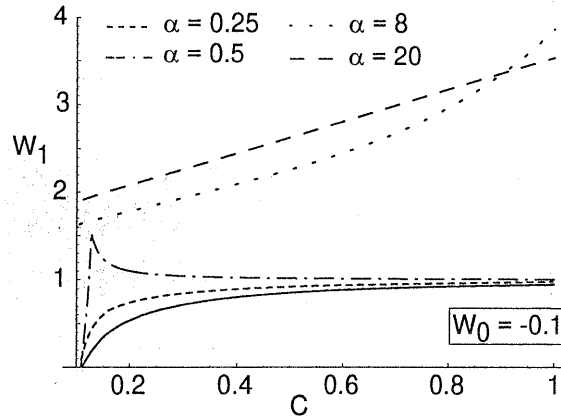
Figure 8: Phase boundary in the (C, W_1) plane between a stable synchronous state and a marginal state of a symmetric two-population IF network. Boundary curves are shown for $W_0 = -0.1$ and various values of the inverse rise time α. The solid curve corresponds to the analog model, whereas the dashed curves correspond to the IF model.

ϕ-dependent variations in the mean firing rates $a(\phi)$, as shown in Figure 9. However, as α is increased, the system bifurcates to a state with periodic or quasiperiodic fluctuations of the ISIs on spatially separated invariant circles (see Figure 10b). Although the average behavior is still consistent with that found in the corresponding analog model, the additional fine structure associated with these orbits is not resolved by the analog model. In order to characterize the size of the ISI fluctuations, we define a deterministic coefficient of variation $C_V(\phi)$ for a neuron ϕ according to

$$C_V(\phi) = \frac{\sqrt{\overline{\left(\Delta(\phi) - \overline{\Delta}(\phi)\right)^2}}}{\overline{\Delta}(\phi)}, \tag{4.17}$$

with averages defined by equation 4.16.

The $C_V(\phi)$ is plotted as a function of ϕ for various values of α in Figure 11a. This shows that the relative size of the deterministic fluctuations in the mean firing rate is an increasing function of α. For slow synapses ($\alpha \to 0$), the C_V is very small, indicating an excellent match between the IF and analog models. However, the fluctuations become much more significant when the synapses are fast. This is further illustrated in Figure 11b, where we plot the variance of the ISIs against the mean. The variance increases monotonically with the mean, which shows why groups of neurons close
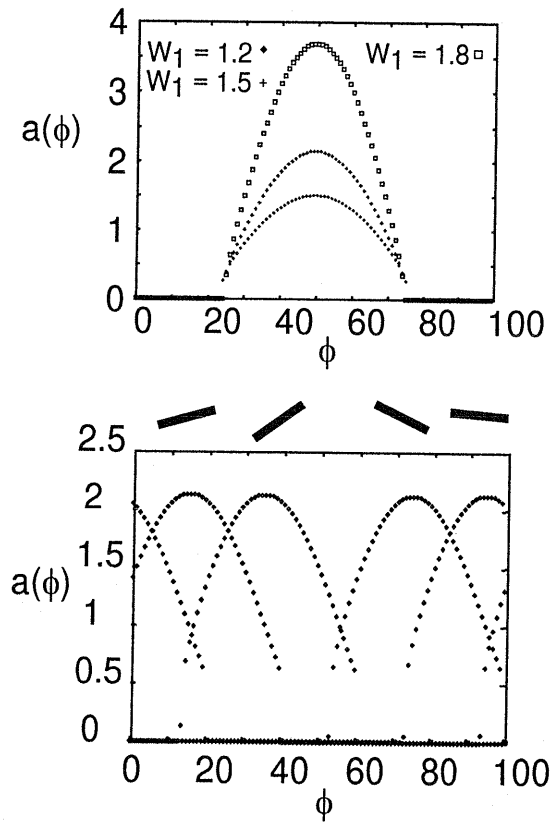
Figure 9: Sharp orientation tuning curves for a symmetric two-population IF network ($N = 100$) and cosine weight kernel. (a) The mean firing rate $a(\phi)$ is plotted as a function of orientation preference ϕ and various W_1. Same parameter values as Figure 3a. (b) Locking to a slowly rotating, weakly tuned external stimulus. Same parameters as Figure 3b.

to the edge of the activity profile in Figure 11a (so that the mean firing rate is relatively small) have a larger C_V. An interpretation of this behavior is that neurons with a low firing rate are close to threshold (i.e., there is an approximate balance between excitation and inhibition), which means that these neurons are more sensitive to fluctuations. Another observation from Figure 11b is that the fluctuations decrease with the size of the network; this appears to be a finite-size effect since there is only a weak dependence on N for $N > 200$.
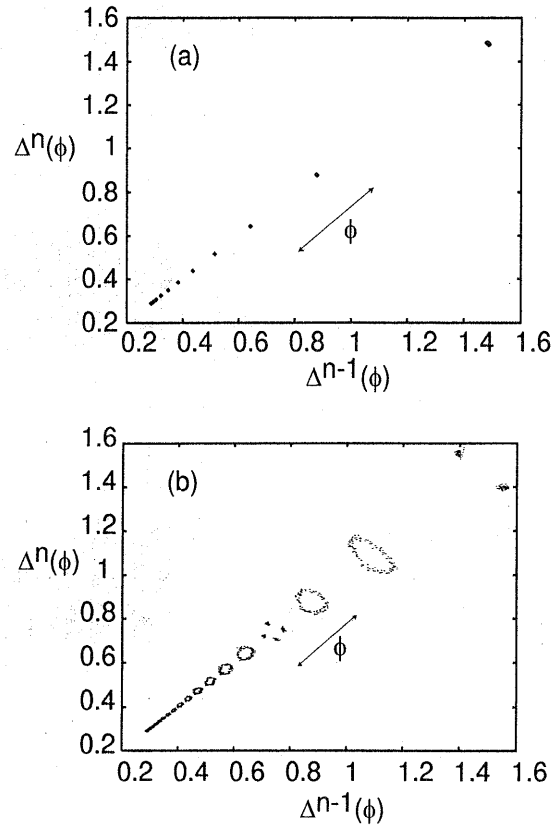
Figure 10: Separation of the ISI orbits for a symmetric two-population IF network ($N = 100$) with $W_0 = -0.5$, $W_1 = 2.0$, $C = 0.25$. (a) $\alpha = 2$. (b) $\alpha = 5$. The (projected) attractors of the ISI pairs with coordinates $(\Delta^{n-1}(\phi), \Delta^n(\phi))$ are shown for all excitatory neurons.

In Figure 12 we plot $(\Delta^{n-1}(\phi), \Delta^n(\phi))$ for two selected neurons: one with a low C_V/fast firing rate and the other with a high C_V/low firing rate. Results are shown for $\alpha = 8$ and $\alpha = 20$. Corresponding ISI histograms are presented in Figure 13. These figures establish that for fast synapses, the ISIs display highly irregular orbits with the invariant circles of Figure 10b no longer present. An interesting question that we hope to pursue elsewhere concerns whether the underlying attractor for the ISIs supports chaotic dynamics, for it is well known that the breakup of invariant circles is one possible route to chaos, as has previously been demonstrated in a num-
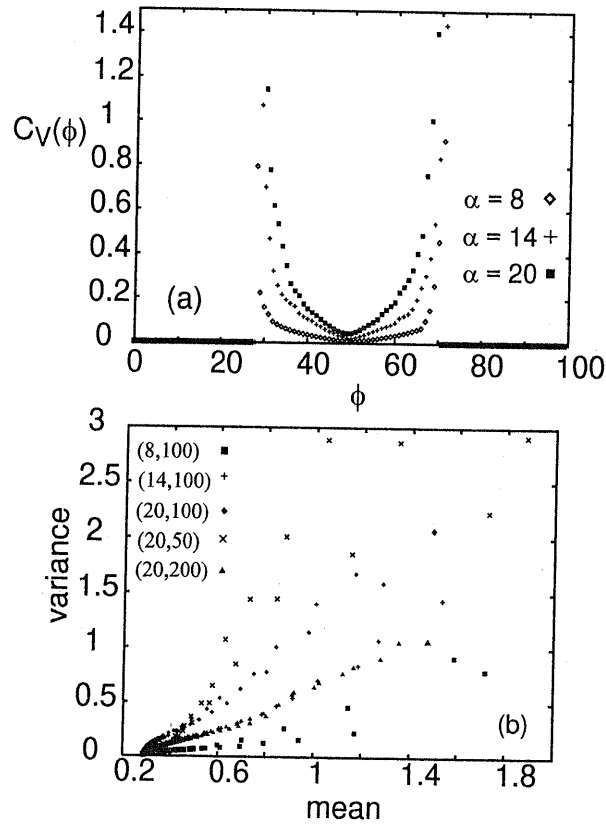
Figure 11: (a) Plot of the coefficient of variation $C_V(\phi)$ as a function of ϕ for various values of the inverse rise time α. (b) Plot of variance against the mean of the ISIs for various values of inverse rise time α and network size N. All other parameter values are as in Figure 10.

ber of classical fluid dynamics experiments (Bergé, Dubois, & Vidal, 1986). As partial evidence for chaotic ISI dynamics, we plot the power spectrum $|h(p)|^2$ of a neuron with high C_V in Figure 14. We consider a sequence of ISIs over $M + 1$ firing events $\{\Delta_k, k = 1, \ldots M\}$ and define

$$h(p) = \frac{1}{\sqrt{M}} \sum_{k=1}^{M} e^{2\pi\, ikp} \Delta_k, \qquad (4.18)$$

where $p = m/M$ for $m = 1, \ldots, M$. Although the numerical data are rather
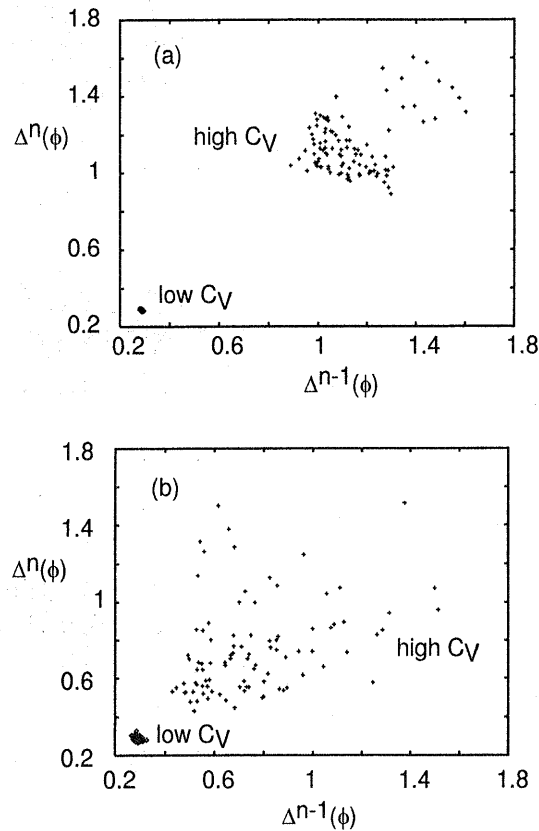
Figure 12: Same as Figure 10 except that (a) $\alpha = 8$ and (b) $\alpha = 20$. The attractor is shown for two excitatory neurons: one with a low C_V and the other with a high C_V.

noisy, it does appear that there is a major difference between the quasiperiodic regime shown in Figure 10 and the high-C_V regime of Figure 12. The latter possesses a broadband spectrum, which is indicative of (but not conclusive evidence for) chaos.

There is currently considerable interest in possible mechanisms for the generation of high C_Vs in networks of cortical neurons. This follows the recent observation by Softky and Koch (1993) of high variability of the ISIs in data from cat V1 and MT neurons. Such variability is inconsistent with the standard notion that a neuron integrates over a large number of small
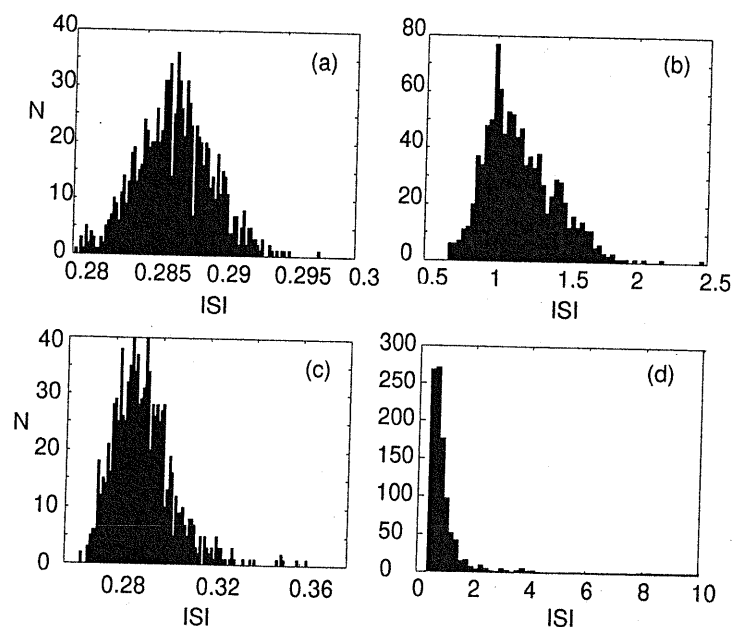
Figure 13: Histograms of 1000 firing events for selected excitatory neurons in a symmetric two-population IF network: (a) $\alpha = 8$, low C_V. (b) $\alpha = 8$, high C_V. (c) $\alpha = 20$, low C_V. (d) $\alpha = 20$, high C_V. All other parameter values are as in Figure 10.

(excitatory) inputs, since this would lead to a regular firing pattern (as a consequence of the law of large numbers). Two alternative approaches to resolving this dilemma have been proposed. The first treats cortical neurons as coincidence detectors that fire in response to a relatively small number of excitatory inputs arriving simultaneously at the (sub)millisecond level—a suggested mechanism for the amplification of a neuron's response is active dendrites (Softky & Koch, 1993). The second approach retains the picture of a neuron as a synaptic integrator by incorporating a large number of inhibitory inputs to balance the effects of excitation so that a neuron operates close to threshold (Usher et al., 1994; Tsodyks & Sejnowski, 1995; van Vreeswijk & Sompolinsky, 1996, 1998). These latter studies incorporate a degree of randomness into a network either in the form of quenched disorder in the coupling or through synaptic noise (see also Lin, Pawelzik, Ernst, & Sejnowski, 1998). We have shown that even an ordered network evolving deterministically can support large fluctuations in the ISIs provided that the synapses are sufficiently fast. For the activity profile shown in Figure 11a,
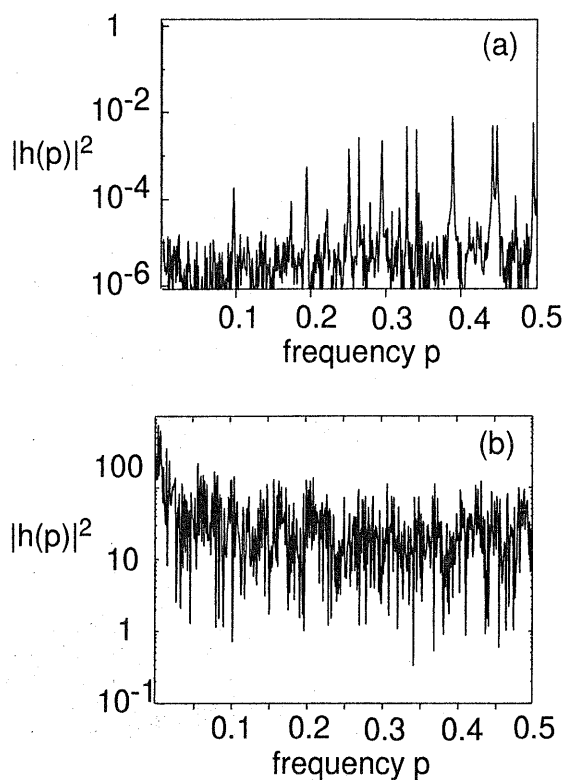
Figure 14: (a) Spectrum of a neuron in the quasiperiodic regime ($\alpha = 5$). (b) Spectrum of a high-C_V neuron with $\alpha = 20$. All other parameter values are as in Figure 10.

only a subset of neurons have a C_V close to unity. In order to achieve a consistently high C_V across the whole network, it is likely that one would need to take into account various sources of disorder present in real biological networks.

5 Intrinsic Traveling Wave Profiles

So far we have restricted our analysis of orientation tuning to the case of a symmetric two-population model in which the excitatory and inhibitory populations behave identically. Sharp orientation tuning can still occur if the symmetry conditions 3.8 are no longer imposed, provided that the first harmonic eigenmodes are excited when the homogeneous resting state is

destabilized ($n = 1$ in equation 3.3 or 4.9). Now, however, the heights of the excitatory and inhibitory activity profiles will generally differ. More significant, it is possible for traveling wave profiles to occur even in the absence of a rotating external stimulus (Ben Yishai et al., 1997). In order to illustrate this phenomenon, suppose that equation 3.7 is replaced by the conditions

$$C_L = C, \quad W_0 = \begin{pmatrix} W_0^E & -W_0^I \\ W_0^E & -W_0^I \end{pmatrix}, \quad W_1 = \begin{pmatrix} W & -K \\ K & -W \end{pmatrix} \tag{5.1}$$

with $K > W$ and $W_n^{LM} = 0$ for all $n \geq 2$. First consider the analog model analyzed in section 3. Under the conditions 5.1, the fixed-point equation 3.1 has solutions $\overline{X}_L = \overline{X}, L = E, I$, where $\overline{X} = W_0 f(\overline{X}) + C$ with $W_0 = W_0^E - W_0^I$. Linearization about this fixed point again yields the eigenvalue equation 3.8, with the eigenvalues of the weight matrices W_n of equation 5.1 now given by

$$\lambda_0^+ = W_0, \quad \lambda_0^- = 0, \quad \lambda_1^\pm = \pm i W_1, \quad W_1 \equiv \sqrt{K^2 - W^2}. \tag{5.2}$$

Equations 3.8 and 5.2 imply that the fixed point $\overline{X}$ is stable with respect to excitation of the $n = 0$ modes provided that $\gamma W_0 < 1$. On the other hand, substituting for $\lambda_2^\pm$ using equation 5.2 shows that there exist solutions for ν of the form

$$\frac{\nu}{\alpha} = -1 + \sqrt{\frac{\gamma W_1}{2}}(1 \pm i). \tag{5.3}$$

Hence, at a critical coupling $W_1 = W_{1c} \equiv 2/\gamma$, the fixed point undergoes a Hopf bifurcation due to the occurrence of a pair of pure imaginary eigenvalues $\nu = \pm i\alpha$. The excited modes take the form $Z^\pm e^{i(2\phi \pm \alpha t)}$, where $Z^\pm$ are the eigenvectors associated with $\lambda_2^\pm$ and correspond to traveling wave activity profiles with rotation frequency α.

Let us now turn to the case of the IF model analyzed in section 4. Linear stability analysis of the synchronous state generates the eigenvalue equation 4.13 with $\lambda_n^\pm$ given by equation 5.2. Following similar arguments to section 3, it can be established that the synchronous state is stable in the weak coupling regime provided that $W_0 < 0$. It is also stable with respect to excitations of the $n = 0$ modes for arbitrary coupling strength. Therefore, we look for strong coupling instabilities of the synchronous state by substituting $\nu = i\omega$ in equation 4.13 for $n = 2$. Equating real and imaginary parts then leads to the pair of equations

$$A_T[\cos(\omega) - 1] = W_1\widetilde{S}(\omega) - W_0\widetilde{C}(0), \quad A_T\sin(\omega) = W_1\widetilde{C}(\omega). \tag{5.4}$$
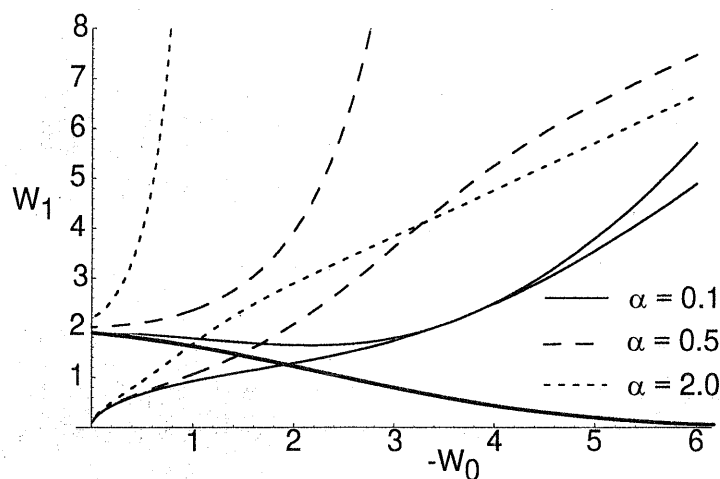
Figure 15: Phase boundary in the (W_0, W_1) plane between a stable synchronous state and a traveling marginal state of an asymmetric two-population IF network. Boundary curves are shown for $C = 0.25$ and various values of the inverse rise time α. For each α there are two solution branches, the lower one of which determines the point of instability of the synchronous state. The boundary curve for the analog model is also shown (thick line).

Examples of boundary curves are shown in Figure 15 for W_1 as a function of W_0 with α fixed. For each α, there are two solution branches, the lower one of which determines the point at which the synchronous state destabilizes. At first sight it would appear that there is a discrepancy between the IF and analog models, for the lower boundary curves of the IF model do not coincide with the phase boundary of the analog model even in the limit $\alpha \to 0$ and $W_0 \to 0$. (Contrast Figure 15 with Figure 8, for example.) However, numerical simulations reveal that as the lower boundary curve of the IF model is crossed from below, the synchronous state destabilizes to a state consisting of two distinct synchronized populations—one excitatory and the other inhibitory. The latter state itself destabilizes for values of W_1 beyond the upper boundary curve, leading to the formation of an intrinsically rotating orientation tuning curve. In Figure 16 we plot the spike train of one of the IF neurons associated with such a state. The neuron clearly exhibits approximately periodic bursts at an angular frequency $\Omega \approx \pi/6\tau_0$, where the time constant τ_0 is the fundamental unit of time. This implies that orientation selectivity can shift over a few tens of milliseconds, an effect that has recently been observed by Ringach et al. (1997).
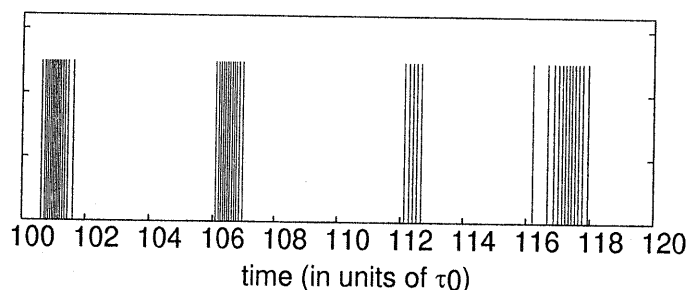
Figure 16: Oscillating spike train of an excitatory neuron in a traveling marginal state of an asymmetric two-population IF network. Here $W_0 = -1.0$, $W_1 = 4.2$, $W_0^{EE} = 42.5$, $W_1^{EE} = 20.0 = J$, $N = 50$, $C = 1.0$, and $\alpha = 2.0$.

6 Discussion

Most analytical treatments of network dynamics in computational neuro-science are based on analog models in which the output of a neuron is taken to be a mean firing rate (interpreted in terms of either population or time averaging). Techniques such as linear stability analysis and bifurcation theory are used to investigate strong coupling instabilities in these networks, which induce transitions to states with complex spatiotemporal activity patterns (see Ermentrout, 1998, for a review). Often a numerical comparison is made with the behavior of a corresponding network of spiking neurons based on the IF model or, perhaps, a more detailed biophysical model such as Hodgkin-Huxley. Recently Bressloff and Coombes (2000) developed analytical techniques for studying strong coupling instabilities in IF networks allowing a more direct comparison with analog networks to be made. We have applied this dynamical theory of strongly coupled spiking neurons to a simple computational model of sharp orientation tuning in a cortical hypercolumn. A number of specific results were obtained that raise interesting issues for further consideration.

- Just as in the analog model, bifurcation theory can be used to study orientation tuning in the IF model. The main results are similar in that the coefficients of the interaction function $W(\phi) = W_0 + 2W_1 \cos(2\phi)$ play a key role in determining orientation tuning. If the cortical interaction is weak—both W_0 and W_1 small—then, as may be expected, only biases in the geniculocortical map can give rise to orientation tuning. However, if W_1 is sufficiently large, then only a weak geniculocortical bias is needed to produce sharp orientation tuning at a given orientation.

- Such a tuning is produced via a subcritical bifurcation, which implies that the switching on and off of cortical cells should exhibit hysteresis (Wilson & Cowan, 1972, 1973). Thus, both tuned and untuned states could coexist under certain circumstances, in both the analog and the IF model. It is of interest that contrast and orientation-dependent hysteresis has been observed in simple cells by Bonds (1991).

- Strong coupling instabilities in the IF model involve a discrete Hopf or period doubling bifurcation in the firing times. This typically leads to non-phase-locked behavior characterized by clustered but irregular variations of the ISIs. These clusters are spatially separated in phase-space, which results in a localized activity pattern for the mean firing rates across the network that is modulated by fluctuations in the instantaneous firing rate. The latter can generate C_Vs of order unity. Moreover, for fast synapses, the underlying attractor for the ISIs as illustrated in Figure 12 appears to support chaotic dynamics. Evidence for chaos in disordered (rather than ordered) balanced networks has been presented elsewhere (van Vreeswijk & Sompolinsky, 1998), although caution has to be taken in ascribing chaotic behavior to potentially high-dimensional dynamical systems. Another interesting question is to what extent the modulations of mean firing rate observed in the responses of some cat cortical neurons to visual stimuli by Gray and Singer (1989) can be explained by discrete bifurcations of the firing times in a network of spiking neurons.

- In cases where the excitatory and inhibitory populations comprising the ring are not identical, traveling wave profiles can occur in response to a fixed stimulus. This implies that peak orientation selectivity can shift over a few tens of milliseconds. Such an effect has been observed by Ringach et al. (1997) and again occurs in both the analog and IF models.

- Certain care has to be taken in identifying parameter regimes over which particular forms of network operation occur, since phase diagrams constructed for analog networks differ considerably from those of IF networks (see Figure 8). For example, good quantitative agreement between the localized activity profiles of the IF and analog models holds only when there is an approximate balance in the mean excitatory and inhibitory coupling and the synaptic interactions are sufficiently slow.

Appendix A _____

Let $X(\phi, t) = \overline{X}$ be a homogeneous fixed point of the one-population model described by equation 3.9, which we rewrite in the more convenient form:

$$\frac{1}{\alpha^2} \frac{\partial^2 X(\phi, t)}{\partial t^2} + \frac{2}{\alpha} \frac{\partial X(\phi, t)}{\partial t} + X(\phi, t)$$

$$= \int_0^\pi \frac{d\phi'}{\pi} W(\phi - \phi') f(X(\phi', t)) + C. \tag{A.1}$$

Suppose that the weight distribution $W(\phi)$ is given by

$$W(\phi) = W_0 + 2 \sum_{k=1}^{\infty} W_k \cos(2k\phi). \tag{A.2}$$

Expand the nonlinear firing-rate function about the fixed point $\overline{X}$ as in equation 3.11. Define the linear operator

$$\hat{L}X = \frac{1}{\alpha^2} \frac{\partial^2 X}{\partial t^2} + \frac{2}{\alpha} \frac{\partial X}{\partial t} + X - \gamma W * X \tag{A.3}$$

in terms of the convolution $W * X(\phi) = \int_0^\pi W(\phi - \phi') X(\phi') d\phi'/\pi$. The operator $\hat{L}$ has a discrete spectrum with eigenvalues ν satisfying (cf. equation 3.7)

$$\left(1 + \frac{\nu}{\alpha}\right)^2 = \gamma W_k \tag{A.4}$$

and corresponding eigenfunctions

$$X(\phi, t) = z_k e^{2ik\phi} + z_k^* e^{-2ik\phi}. \tag{A.5}$$

Suppose that W_n for some $n \neq 0$ is chosen as a bifurcation parameter and $\gamma W_k < 1$ for all $k \neq n$. Then $W_n = W_{n,c} \equiv \gamma^{-1}$ is a bifurcation point for destabilization of the homogeneous state $\overline{X}$ due to excitation of the nth modes. Set $W_n - W_{nc} = \epsilon^2$, $W_c(\phi) = W(\phi)|_{W_n = W_{n,c}}$, and perform the following perturbation expansion:

$$X = \overline{X} + \epsilon X_1 + \epsilon^2 X_2 + \cdots \tag{A.6}$$

Introduce a slow timescale $\tau = \epsilon^2 t$ and collect terms with equal powers of

ϵ. This leads to a hierarchy of equations of the form

$$\mathcal{O}(1): \quad \overline{X} = W_0\, f(\overline{X}) + C \tag{A.7}$$

$$\mathcal{O}(\epsilon): \quad \hat{L}_c X_1 = 0 \tag{A.8}$$

$$\mathcal{O}(\epsilon^2): \quad \hat{L}_c X_2 = g_2 W_c * X_1^2 \tag{A.9}$$

$$\mathcal{O}(\epsilon^3): \quad \hat{L}_c X_3 = g_3 W_c * X_1^3 + 2g_2 W_c * X_1 X_2 - \left[\frac{2}{\alpha}\frac{\partial X_1}{\partial \tau} - \gamma f_n * X_1 \right], \tag{A.10}$$

where $\hat{L}_c = X - \gamma W_c * X$ and $f_n(\phi) = \cos(2n\phi)$. The $\mathcal{O}(1)$ equation determines the fixed point $\overline{X}$. The $\mathcal{O}(\epsilon)$ equation has solutions of the form

$$X_1(\phi, t) = z(\tau)\, e^{2in\phi} + z^*(\tau)\, e^{-2in\phi}. \tag{A.11}$$

We shall determine a dynamical equation for the complex amplitude $z(\tau)$ by deriving so-called solvability conditions for the higher-order equations.

We proceed by taking the inner product of equations A.9 and A.10 with the linear eigenmode A.11. We define the inner product of two periodic functions U, V according to $\langle U|V\rangle = \int_0^\pi U^*(\phi)V(\phi)d\phi/\pi$. The $\mathcal{O}(\epsilon^2)$ solvability condition $\langle X_1|\hat{L}_c X_2\rangle = 0$ is automatically satisfied since

$$\langle X_1|W_c * X_1^2\rangle = 0. \tag{A.12}$$

The $\mathcal{O}(\epsilon^3)$ solvability condition $\langle X_1|\hat{L}_c X_3\rangle = 0$ gives

$$\langle X_1|\frac{2}{\alpha}\frac{\partial X_1}{\partial \tau} - W_c * X_1\rangle = g_3\langle X_1|W_c * X_1^3\rangle + 2g_2\langle X_1|W_c * X_1 X_2\rangle. \tag{A.13}$$

First, we have

$$\langle e^{2in\phi}|\frac{2}{\alpha}\frac{\partial X_1}{\partial \tau} - \gamma f_n * X_1\rangle = \frac{2}{\alpha}\frac{dz}{d\tau} - \gamma z \tag{A.14}$$

and

$$\langle e^{2in\phi}|W_c * X_1^3\rangle = W_{n,c}\int_0^\pi \frac{d\phi}{\pi}\left(ze^{2in\phi} + z^*e^{-2in\phi}\right)^3 e^{-2in\phi}$$

$$= 3 W_{n,c} z|z|^2. \tag{A.15}$$

The next step is to determine U_2. From equation A.9 we have

$$U_2(\phi) - \gamma \int_0^\pi \frac{d\phi'}{\pi} W_c(\phi - \phi') U_2(\phi')$$

$$= g_2 \int_0^\pi \frac{d\phi'}{\pi} W_c(\phi - \phi') U_1(\phi')^2$$

$$= g_2 \left[z^2 W_{2n} e^{4in\phi} + z^{*2} W_{2n} e^{-4in\phi} + 2|z|^2 W_0 \right]. \tag{A.16}$$

Let

$$X_2(\phi) = V_+ e^{4in\phi} + V_- e^{-4in\phi} + V_0 + \kappa X_1(\phi). \tag{A.17}$$

The constant κ remains undetermined at this order of perturbation but does not appear in the amplitude equation for $z(\tau)$. Substituting equation A.17 into A.16 yields

$$V_+ = \frac{g_2 z^2 W_{2n}}{1 - \gamma W_{2n}}, \quad V_- = \frac{g_2 z^{*2} W_{2n}}{1 - \gamma W_{2n}}, \quad V_0 = \frac{2g_2 W_0}{1 - \gamma W_0}. \tag{A.18}$$

Using equation A.18, we find that

$$\langle e^{2in\phi} | W_c * X_1 X_2 \rangle = W_{n,c} \int_0^\pi \frac{d\phi}{\pi} \left(z e^{2in\phi} + z^* e^{-2in\phi} \right)$$

$$\times \left(V_+ e^{4in\phi} + V_- e^{-4in\phi} + V_0 + \kappa X_1(\phi) \right) e^{-2in\phi}$$

$$= W_{n,c}[z^* V_+ + z V_0]$$

$$= g_2 W_{n,c} z |z|^2 \left[\frac{W_{2n}}{1 - \gamma W_{2n}} + \frac{2 W_0}{1 - \gamma W_0} \right]. \tag{A.19}$$

Combining equations A.14, A.15, and A.19, we obtain the Stuart-Landau equation,

$$\frac{dz}{d\tau} = z(1 + A|z|^2), \tag{A.20}$$

where we have absorbed a factor $\gamma\alpha/2$ into τ and

$$A = \frac{3g_3}{\gamma^2} + \frac{2g_2^2}{\gamma^2} \left[\frac{W_{2n}}{1 - \gamma W_{2n}} + \frac{2 W_0}{1 - \gamma W_0} \right]. \tag{A.21}$$

After rescaling, $\epsilon z = Z$, $\tau = \epsilon^2 t$, this becomes

$$\frac{dZ}{dt} = Z(W_n - W_{n,c} + A|Z|^2). \tag{A.22}$$

Appendix B

In this appendix we write explicit expressions for various quantities evaluated in the particular case of the alpha function 2.8. First, the phase interaction function defined by equation 4.2 becomes

$$K_T(\phi) = \frac{\alpha^2}{1-\alpha} \frac{1-e^{-T}}{1-e^{-\alpha T}} \left[a_1(T)e^{-\alpha T\phi} + T\phi e^{-\alpha T\phi} + a_2(T)e^{-T\phi} \right] \quad (B.1)$$

$$a_1(T) = \frac{Te^{-\alpha T}}{1-e^{-\alpha T}} - \frac{1}{1-\alpha}, \quad a_2(T) = \frac{1}{1-\alpha} \frac{1-e^{-\alpha T}}{1-e^{-T}}. \quad (B.2)$$

Second, equations 2.8 and 4.7 give

$$\widetilde{G}_T(\nu) = \frac{F_0(T)}{1-e^{-\alpha T-\nu}} - \frac{F_1(T)e^{-\alpha T-\nu}}{(1-e^{-\alpha T-\nu})^2}, \quad (B.3)$$

where

$$F_0(T) = \frac{\alpha^2 e^{-T}}{(1-\alpha)^2} \left[(1-\alpha T+\alpha^2 T)e^{(1-\alpha)T} - 1 \right] \quad (B.4)$$

$$F_1(T) = \frac{T\alpha^3 e^{-T}}{1-\alpha} \left[e^{(1-\alpha)T} - 1 \right]. \quad (B.5)$$

Finally, setting $\nu = i\omega$ in equation B.3 and taking real and imaginary parts leads to the result

$$\widetilde{C}(\omega) = a(\omega)C(\omega)$$
$$- b(\omega)\left(\cos(\omega)[C(\omega)^2 - S(\omega)^2] - 2\sin(\omega)C(\omega)S(\omega) \right) \quad (B.6)$$

$$\widetilde{S}(\omega) = a(\omega)S(\omega)$$
$$- b(\omega)\left(\sin(\omega)[C(\omega)^2 - S(\omega)^2] + 2\cos(\omega)C(\omega)S(\omega) \right) \quad (B.7)$$

where

$$a(\omega) = \frac{F_0(T)}{C(\omega)^2 + S(\omega)^2}, \quad b(\omega) = \frac{F_1(T)e^{-\alpha T}}{[C(\omega)^2 + S(\omega)^2]^2} \quad (B.8)$$

and $C(\omega) = 1 - e^{-\alpha T}\cos(\omega)$, $S(\omega) = e^{-\alpha T}\sin(\omega)$.

Acknowledgments

References

Amit, D. J., & Tsodyks, M. V. (1991). Quantitative study of attractor neural networks retrieving at low spike rates I: Substrate-spikes, rates and neuronal gain. *Network, 2,* 259–274.

Ben-Yishai, R., Bar-Or Lev, R., & Sompolinsky, H. (1995). Theory of orientation tuning in visual cortex. *Proc. Natl. Acad. Sci. (USA), 92,* 3844–3848.

Ben-Yishai, R., Hansel, D., & Sompolinsky, H. (1997). Traveling waves and the processing of weakly tuned inputs in a cortical network module. *J. Comput. Neurosci., 4,* 57–77.

Bergé, P., Dubois, M., & Vidal, C. (1986). *Order within chaos.* New York: Wiley.

Bonds, A. B. (1991). Temporal dynamics of contrast gain control in single cells of the cat striate cortex. *Visual Neuroscience, 6,* 239–255.

Bressloff, P. C., & Coombes, S. (1997). Physics of the extended neuron. *Int. J. Mod. Phys., 11,* 2343–2392.

Bressloff, P. C., & Coombes, S. (1998a). Desynchronization, mode-locking and bursting in strongly coupled IF oscillators. *Phys. Rev. Lett., 81,* 2168–2171.

Bressloff, P. C., & Coombes, S. (1998b). Spike train dynamics underlying pattern formation in integrate-and-fire oscillator networks. *Phys. Rev. Lett., 81,* 2384–2387.

Bressloff, P. C., & Coombes, S. (2000). Dynamics of strongly coupled spiking neurons. *Neural Comput., 12,* 91–129.

Chapman, B., Zahs, K. R., & Stryker, M. P. (1991). Relation of cortical cell orientation selectivity to alignment of receptive fields of the geniculocortical afferents that arborize within a single orientation column in ferret visual cortex. *J. Neurosci., 11,* 1347–1358.

Cowan, J. D. (1968). Statistical mechanics of nervous nets. In E. R. Caianiello (Ed.), *Neural networks* (pp. 181–188). Berlin: Springer-Verlag.

Cowan, J. D. (1982). Spontaneous symmetry breaking in large scale nervous activity. *Int. J. Quantum Chem., 22,* 1059–1082.

Cross, M. C., & Hohenberg, P. C. (1993). Pattern formation outside of equilibrium. *Rev. Mod. Phys., 65,* 851–1112.

Destexhe, A., Mainen, A. F., & Sejnowski, T. J. (1994). Synthesis of models for excitable membranes synaptic transmission and neuromodulation using a common kinetic formalism. *J. Comp. Neurosci., 1,* 195–231.

Dimitrov, A., & Cowan, J. D. (1998). Spatial decorrelations in orientation-selective cells. *Neural Comput., 10,* 1779–1796.

Douglas, R. J., Koch, C., Mahowald, M., Martin, K., & Suarez, H. (1995). Recurrent excitation in neocortical circuits. *Science, 269,* 981–985.

Ermentrout, G. B. (1998). Neural networks as spatial pattern forming systems. *Rep. Prog. Phys., 61,* 353–430.

Ermentrout, G. B., & Cowan, J. D. (1979a). A mathematical theory of visual hallucination pattens. *Biol. Cybern., 34*, 137–150.

Ermentrout, G. B., & Cowan, J. D. (1979b). Temporal oscillations in neuronal nets. *J. Math. Biol., 7*, 265–280.

Ferster, D., Chung, S., & Wheat, H. (1997). Orientation selectivity of thalamic input to simple cells of cat visual cortex. *Nature, 380*, 249–281.

Ferster, D., & Koch, C. (1987). Neuronal connections underlying orientation selectivity in cat visual cortex. *Trends in Neurosci., 10*, 487–492.

Georgopolous, A. P. (1995). Current issues in directional motor control. *Trends in Neurosci., 18*, 506–510.

Gerstner, W., van Hemmen, J. L., & Cowan, J. D. (1996). What matters in neuronal locking. *Neural Comput., 94*, 1653–1676.

Gray, C. M., & Singer, W. (1989). Stimulus-specific neuronal oscillations in orientation columns of cat visual cortex. *Proc. Nat. Acad. Sci., 86*, 1698–1702.

Hansel, D., & Sompolinsky, H. (1996). Chaos and synchrony in a model of a hypercolumn in visual cortex. *J. Comput. Neurosci., 3*, 7–34.

Hansel, D., & Sompolinsky, H. (1997). Modeling feature selectivity in local cortical circuits. In C. Koch & I. Segev (Eds.), *Methods of neuronal modeling* (2nd ed.) (pp. 499–567). Cambridge, MA: MIT Press.

Hubel, D. H., & Wiesel, T. N. (1962). Receptive fields, binocular interaction and functional architecture in the cat's visual cortex. *J. Physiol. Lond., 160*, 106–154.

Jack, J. J. B., Noble, D., & Tsien, R. W. (1975). *Electric current flow in excitable cells.* Oxford: Clarendon Press.

Lin, J. K., Pawelzik, K., Ernst, U., & Sejnowski, T. J. (1998). Irregular synchronous activity in stochastically-coupled networks of integrate-and-fire neurons. *Network: Comput. Neural Syst., 9*, 333–344.

Lukashin, A. V., & Georgopolous, A. P. (1994a). A neural network for coding trajectories by time series of neuronal population vectors. *Neural Comput., 4*, 57–77.

Lukashin, A. V., & Georgopolous, A. P. (1994b). Directional operations in the motor cortex modeled by a neural network of spiking neurons. *Biol. Cybern., 71*, 79–85.

Mundel, T., Dimitrov, A., & Cowan, J. D. (1997). Visual cortex circuitry and orientation tuning. In M. Mozer, M. Jordan, & T. Petsche (Eds.), *Advances in neural information processing systems, 9* (pp. 887–893). Cambridge, MA: MIT Press.

Murray, J. D. (1990). *Mathematical biology.* Berlin: Springer-Verlag.

Nelson, S., Toth, L., Seth, B., & Mur, S. (1994). Orientation selectivity of cortical neurons during extra-cellular blockade of inhibition. *Science, 265*, 774–777.

Pei, X., Vidyasagar, T. R., Volgushev, M., & Creutzseldt, O. D. (1994). Receptive field analysis and orientation selectivity of postsynaptic potentials of simple cells in cat visual cortex. *J. Neurosci., 14*, 7130–7140.

Pinto, D. J., Brumberg, J. C., Simons, D. J., & Ermentrout, G. B. (1996). A quantitative population model of whisker barrels: Re-examining the Wilson-Cowan equations. *J. Comput. Neurosci., 6*, 19–28.

Reid, R. C., & Alonso, J. M. (1995). Specificity of monosynaptic connections from thalamus to visual cortex. *Nature, 378*, 281–284.

Ringach, D., Hawken, M. J., & Shapley, R. (1997). Dynamics of orientation tuning in macaque primary visual cortex. *Nature, 387*, 281–284.

Sillito, A. M., Kemp, J. A., Milson, J. A., & Beradi, N. (1980). A re-evaluation of the mechanisms underlying simple cell orientation selectivity. *Brain Res., 194*, 517–520.

Softky, W. R., & Koch, C. (1993). The highly irregular firing of cortical cells is inconsistent with temporal integration of random EPSPs. *J. Neurosci., 13*, 334-350.

Somers, D. C., Nelson, S. B., & Sur, M. (1995). An emergent model of orientation selectivity in cat visual cortical simple cells. *J. Neurosci., 15*, 5448–5465.

Tsodyks, M. V., & Sejnowski, T. J. (1995). Rapid switching in balanced cortical network models. *Network: Comput. Neural Syst., 6*, 111–124.

Usher, M., Stemmler, M., Koch, C., & Olami, Z. (1994). Network amplification of local fluctuations causes high spike rate variability, fractal firing patterns and oscillatory local field potentials. *Neural Comput., 5*, 795–835.

van Vreeswijk, C. (1996). Partial synchronization in populations of pulse-coupled oscillators. *Phys. Rev. E., 54*, 5522–5537.

van Vreeswijk, C., & Sompolinsky, H. (1996). Chaos in neuronal networks with balanced excitatory and inhibitory activity. *Science, 274*, 1724–1726.

van Vreeswijk, C., & Sompolinsky, H. (1998). Chaotic balanced state in a model of cortical circuits. *Neural Comput., 10*, 1321–1371.

Wilson, H. R., & Cowan, J. D. (1972). Excitatory and inhibitory interactions in localized populations of model neurons. *Biophys. J., 12*, 1–24.

Wilson, H. R., & Cowan, J. D. (1973). A mathematical theory of the functional dynamics of cortical and thalamic nervous tissue. *Kybernetik, 13*, 55–80.

Zhang, K. (1996). Representation of spatial orientation by the intrinsic dynamics of the head-direction cell ensemble: A theory. *J. Neurosci., 16*, 2122–2126.